



HAL
open science

Properties, Extensions and Application of Piecewise Linearization for Euclidean Norm Optimization in R²

Aloïs Duguet, Christian Artigues, Laurent Houssin, Sandra Ulrich Ngueveu

► **To cite this version:**

Aloïs Duguet, Christian Artigues, Laurent Houssin, Sandra Ulrich Ngueveu. Properties, Extensions and Application of Piecewise Linearization for Euclidean Norm Optimization in R². 2021. hal-03356034v1

HAL Id: hal-03356034

<https://hal.science/hal-03356034v1>

Preprint submitted on 27 Sep 2021 (v1), last revised 14 Apr 2023 (v4)

HAL is a multi-disciplinary open access archive for the deposit and dissemination of scientific research documents, whether they are published or not. The documents may come from teaching and research institutions in France or abroad, or from public or private research centers.

L'archive ouverte pluridisciplinaire **HAL**, est destinée au dépôt et à la diffusion de documents scientifiques de niveau recherche, publiés ou non, émanant des établissements d'enseignement et de recherche français ou étrangers, des laboratoires publics ou privés.

Properties, Extensions and Application of Piecewise Linearization for Euclidean Norm Optimization in \mathbb{R}^2

Aloïs Duguet, Christian Artigues, Laurent Houssin, Sandra U. Ngueveu
LAAS-CNRS, Université de Toulouse, CNRS, UPS, INP, France

Abstract

This paper considers non-convex mixed-integer nonlinear programming where nonlinearity comes in the presence of the two-dimensional euclidean norm in the objective or the constraints. We build from the euclidean norm piecewise linearization proposed by [Camino et al., 2019], that allows to solve such non-convex problems via mixed-integer linear programming with an arbitrary approximation guarantee. Theoretical results that make this linearization able to satisfy any given approximation level with the minimum number of pieces are established. An extension of the piecewise linearization approach sharing the same theoretical properties is proposed for elliptic constraints and/or objective. An application of the elliptic linearization to a non-convex beam layout mixed optimization problem coming from an industrial application shows the practical appeal of the approach.

1 Introduction

This paper deals with non-convex mixed-integer non linear programming (MINLP) problems involving euclidean norms either in the objective, the constraints or both. Typical examples are minimization or maximization of distances between objects, as well as convex proximity or separation constraints. Recent applications involve service infrastructure placement in 5G networks [Santoyo-González and Cervelló-Pastor, 2018], relay node deployment in wireless networks [Zhou et al., 2018] and beam layout optimization in telecommunication satellites [Camino et al., 2014, 2019]. We will use the latter problem as a case-study.

MINLP problems are very challenging. Exact methods are generally based on Branch-and-Bound [Smith and Pantelides, 1999] to ensure global optimality, using different relaxations [Nowak, 2005, Adams and Sherali, 1986], for example convex relaxation [Liberti, 2004] or convex envelopes [Tardella, 2007]. To exhibit these relaxations, a large amount of works deals with problem reformulation to simplify the computation of the relaxation or to strengthen it [Liberti,

2004, Liberti et al., 2009b, Serali and Liberti, 2008, Smith and Pantelides, 1999]. A family of reformulation methods commonly used is the reformulation-linearization technique (RLT) [Serali and Liberti, 2008, Serali and Adams, 1999]. Applying this method requires two steps: first, reformulate the problem to add valid nonlinear constraints; second, linearize by replacing variable products by new continuous variables. Generally, MINLP problems are considered harder to solve than Mixed-Integer Linear Programming (MILP) ones, leading to the use of reformulation methods [Geißler et al., 2012, Liberti et al., 2009a].

Indeed, MILP solvers are often able to tackle industrial-sized problems [Borghetti et al., 2008, Camponogara et al., 2011]. Linearizing a MINLP problem consists in replacing all nonlinear functions of the problem by piecewise linear ones. Theoretical advantages of MINLP linearizations are discussed in [Geißler et al., 2012]. In some cases, there are methods to obtain guarantee on the solution of the linear approximation of the MINLP problem, which gives sense to linearization. However, linearization has also drawbacks like the fastly increasing number of variables and constraints needed to represent a piecewise linear function depending on the dimension of the input [Hughes and Anderson, 1996, Smith, 2000]. Another drawback is the control of the approximation error [Geißler et al., 2012].

Despite those disadvantages, linearization is a widely used method to solve MINLP problems and linearizing methods published are numerous. There are linearizing methods valid for any dimensions in [Geißler et al., 2012, Zhang and Wang, 2008] and for two dimensions or more in [D'Ambrosio et al., 2010, Misener et al., 2009, Rovatti et al., 2014, Silva and Camponogara, 2014].

A particularly relevant topic in linearization is the modeling of a piecewise linear function. Indeed, good properties of formulations have been identified, such as the locally ideal property, which means that every vertex of the linear relaxation is integral [Padberg, 2000, Keha et al., 2004]. A comparison of formulations depending on this property is available in [Sridhar et al., 2013], and a formulation using a number of binary variables and constraints logarithmic in the number of pieces is in [Vielma and Nemhauser, 2011].

Eventually, as MINLP linearization only yield an approximation of the starting problem, being able of quantifying the approximation error is a major advantage. There is at least two general ways of controlling the approximation when the linearization is only in the objective function. The first is a trial and error procedure: linearize the MINLP problem, check the quality of the solution found, and if it is not good enough try to linearize with more pieces to better approximate the nonlinear functions. Despite being an easy linearization scheme, this yields two disadvantages: it is not known when this scheme will stop, and the error is measured only on one point. It is why the second way of linearizing is to enforce before optimisation that the biggest approximation error made by the linearization will be smaller than $\delta > 0$ which means that the optimal value of the approximated MINLP is no more than δ away from the optimal value of the MINLP. Examples of the second way of controlling the approximation error are described in [Rosen and Pardalos, 1986, Dunham, 1986]. Building a piecewise linear bounding of the nonlinear functions is part of the second general way of

controlling the approximation error. Such boundings are used in [Geißler et al., 2012, Rebennack and Kallrath, 2015a, Ngueveu, 2019, Rebennack and Krasko, 2020]. The last property to introduce is that as the number of pieces used in a piecewise linear function increases, the MILP problem associated will require an increasing number of binary variables and constraints, which means that the problem will take longer to be solved. That leads to the goal of using as few pieces as possible to achieve a satisfying approximation error.

This article focuses on using the lowest number of pieces to satisfy a given approximation level rather than minimizing the approximation level with a given number of pieces. To our knowledge, articles in the litterature are few to choose the same point of view [Rosen and Pardalos, 1986, Rebennack and Kallrath, 2015b, Ngueveu, 2019, Rebennack and Krasko, 2020]. The goal of this article is to develop such a linearizing method for the euclidean norm, building on the linearization approach proposed by [Camino et al., 2019].

This article has two main goals : first, to prove that given an approximation level the linearizing method described in [Camino et al., 2019] can be used to obtain a piecewise linear bounding of the euclidean norm of \mathbb{R}^2 that uses the minimal number of pieces. The second goal is to extend this bounding method to other functions while keeping the same properties. In particular we will address the linearization of the elliptic norm that has an application in the telecommunication satellite domain to evaluate the gain obtained by covering user areas with elliptic beams rather than circular ones.

The article is organized as follows: Section 2 describes the euclidean norm linearization of [Camino et al., 2019], and proves that given an approximation level, it creates a piecewise linear bounding with the minimal number of pieces. In section 3, it is shown that the linearizing method of [Camino et al., 2019] can be used to linearize the euclidean norm of \mathbb{R}^2 in the objective function, and that it can be adapted to linearize norm with level set that are ellipses. In section 4, the interest of linearizing elliptic constraints is demonstrated on the beam layout satellite telecommunication problem. Eventually, conclusions are drawn in section 5.

2 Euclidean Norm Linearization

In this section, the linearization scheme of the euclidean norm of \mathbb{R}^2 of [Camino et al., 2019] is described, then the approximation error used all along this article is defined, tailored for the linearization discussed, and finally it is proved that, given an approximation level to respect, the linearization of [Camino et al., 2019] can be used to create a piecewise linear bounding with the minimal number of pieces.

2.1 Method Description

The method of [Camino et al., 2019] describes how to linearize a constraint with the euclidean norm of \mathbb{R}^2 in the form of (1) or (4). However, it cannot be

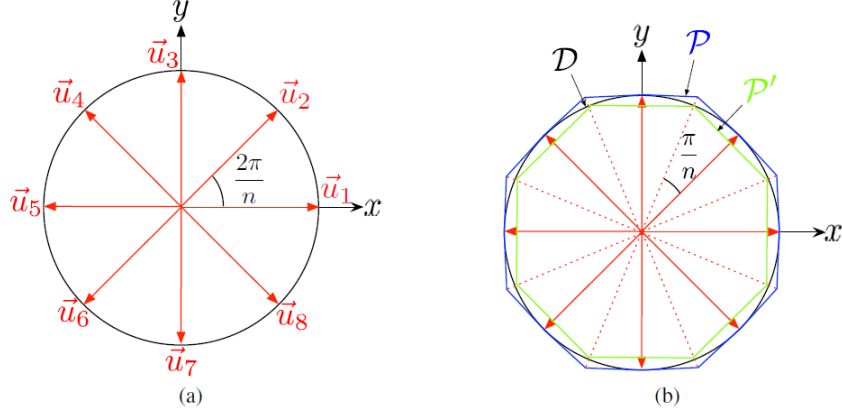


Figure 1: Linearization of the euclidean norm of \mathbb{R}^2 for $P = 8$ directions [Camino et al., 2019]

applied to a sum of euclidean norm. The linearization is based on the evaluation of multiple scalar products between the vector appearing in the euclidean norm and unit vectors regularly spaced out. Let $\|\cdot\|_2$ be the euclidean norm of \mathbb{R}^n . Let us consider constraint (1), for $\Delta \in \mathbb{R}^+$.

$$\|x\|_2 \leq \Delta \quad x \in \mathbb{R}^2 \quad (1)$$

This constraint is satisfied if x is in the centered disk with radius Δ . Set $\mathbf{u}_i = (\cos \frac{2i\pi}{p}, \sin \frac{2i\pi}{p})$ for $i = 1, \dots, p$ with p the number of scalar product that will be used for the linearization. The directions \mathbf{u}_i for $i = 1, \dots, 8$ are depicted in figure 1(a). The linearization consists in replacing (1) by (2), with \cdot being the usual scalar product.

$$x \cdot \mathbf{u}_i \leq \Delta \quad \forall i = 1, \dots, p \quad (2)$$

Throughout this article, the word "polygon" means a solid plane region inside a closed polygonal chain without intersections. A polygonal chain is a union of segments where one segment intersects with the following and the former segment of the chain, and only at its endpoints. In addition, it is closed if the startpoint and the endpoint are the same. If constraint (2) is satisfied, x is in the blue polygon of figure 1(b), and according to [Camino et al., 2019, Proposition 1] another bound on $\|x\|_2$ is known :

$$\|x\|_2 \leq \frac{\Delta}{\cos \frac{\pi}{p}} \quad (3)$$

In addition, if one of the constraints of (2) is not satisfied, x is out of the blue polygon, and [Camino et al., 2019, Proposition 2] gives that :

$$\|x\|_2 \geq \Delta \tag{4}$$

In this example, (2) is a relaxation of (1), thus some x satisfying (2) might be infeasible for (1), but of course a stricter constraint than (1) can be obtained by linearizing it with :

$$x \cdot \mathbf{u}_i \leq \Delta \cos \frac{\pi}{p} \quad \forall i = 1, \dots, p \tag{5}$$

which leads to the green polygon of figure 1(b) being the feasible set of (5).

The linearization of constraint (4) differs from that of (1) because (4) is nonconvex. Thus the big-M technique are used, but the principle stays the same. The linearization is displayed below, where M_i must be a valid upper bound of $\Delta - x \cdot \mathbf{u}_i$ which can be easily obtained as soon as the coordinates are bounded.

$$x \cdot \mathbf{u}_i \geq \Delta - M_i(1 - b_i) \quad \forall i = 1, \dots, p \tag{6}$$

$$\sum_{i=1}^p b_i = 1 \tag{7}$$

$$b_i \text{ binary variable} \quad \forall i = 1, \dots, p \tag{8}$$

Remark that the polygons created by the linearization of (1) into both (2) and (5) are convex regular convex polygons with p sides, for all $p > 3$, because they are both convex, equiangulars and equilaterals. Note that in the rest of this article, regular polygon will be used for convex regular polygon.

A last remark would be that the blue polygon is the "smallest" regular polygon of 8 sides containing the black disk because every segment's middle point touches the circle forming the disk, and that the green polygon is the "biggest" inside the black disk because every vertex touches the circle forming the disk. In the following, the focus is on the approximation of the frontier of constraints of type $\|x\|_2 \leq \Delta$ or $\|x\|_2 \geq \Delta$, and the blue polygon is denoted an *outer approximation* of the disk while the green polygon is denoted an *inner approximation* of the disk. The terms outer approximation and inner approximation as used in this paper are properly defined in the following subsection.

2.2 Approximation Error

An approximation error tailored for the euclidean norm is defined for the study of the linearization of [Camino et al., 2019]. It measures the highest proportion of euclidean norm of two points inside the difference of a disk $B(x_0, \Delta)$ and another set. If the set contains the disk, it is denoted an outer approximation, and if it is included in the disk, it is denoted an inner approximation.

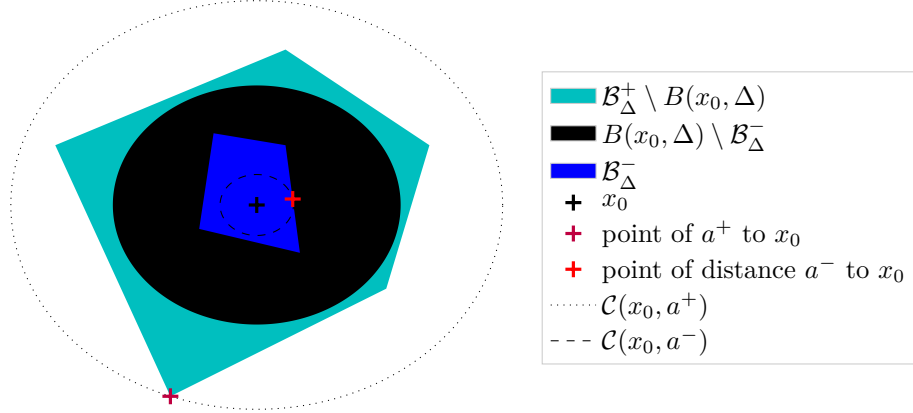


Figure 2: Illustration of definition 2.2

Let $n \in \mathbb{N}^*$ and $x_0 \in \mathbb{R}^n$. Let $B(x_0, \Delta) = \{x \in \mathbb{R}^n : \|x - x_0\|_2 \leq \Delta\}$ be the disk of radius Δ and center x_0 , with $\Delta \in \mathbb{R}^+$.

Let $\mathcal{B}_\Delta^+ \subset \mathbb{R}^n$ and $a^+ \in \mathbb{R}^+$ be such that $B(x_0, \Delta) \subset \mathcal{B}_\Delta^+$ and $a^+ = \max\{\|x - x_0\|_2 : x \in \mathcal{B}_\Delta^+ \setminus B(x_0, \Delta)\}$.

Finally, let $\mathcal{B}_\Delta^- \subset \mathbb{R}^n$ and $a^- \in \mathbb{R}^+$ be such that $\mathcal{B}_\Delta^- \subset B(x_0, \Delta)$ and $a^- = \min\{\|x - x_0\|_2 : x \in B(x_0, \Delta) \setminus \mathcal{B}_\Delta^-\}$.

We note:

- \mathcal{B}_Δ^+ an outer approximation of $B(x_0, \Delta)$ with error $\epsilon := \frac{a^+}{\Delta} - 1$
- \mathcal{B}_Δ^- an of $B(x_0, \Delta)$ with error $\epsilon := \frac{\Delta}{a^-} - 1$
- \mathcal{B}_Δ^+ and \mathcal{B}_Δ^- a bounding of $B(x_0, \Delta)$ with error $\epsilon := \max\{\frac{a^+}{\Delta}, \frac{\Delta}{a^-}\} - 1$

The -1 term in the formula of ϵ is added so that an approximation with error $\epsilon = 0$ is exact. A similar definition can be made for constraints $\|x - x_0\|_2 \geq \Delta$. Figure 2 illustrates the definition. \mathcal{B}_Δ^+ is the region in cyan, black and blue while \mathcal{B}_Δ^- is the region in blue and $B(x_0, \Delta)$ is the black and blue region. The cyan region is $\mathcal{B}_\Delta^+ \setminus B(x_0, \Delta)$, with point of maximal distance from x_0 the purple one, and minimal distance any point on the boundary of $B(x_0, \Delta)$. The black region is $B(x_0, \Delta) \setminus \mathcal{B}_\Delta^-$, with point of minimal distance from x_0 the red one, and maximal norm point any point in the boundary of $B(x_0, \Delta)$.

In this article, \mathcal{B}_Δ^+ (resp. \mathcal{B}_Δ^-) is the set of $x \in \mathbb{R}^2$ satisfying constraints (5) (resp. constraints (2)) or constraints (5) with reversed inequality (resp. constraints (2) with reversed inequality). It is illustrated in figure 3 where the black disk is bounded by the two red squares induced by the linearization of (2) and (5) for $P = 4$. The maximal norm of the outer approximation square (resp. the minimal norm of the inner approximation square) is depicted by the cyan circle (resp. the blue circle). The approximation error is the maximum between

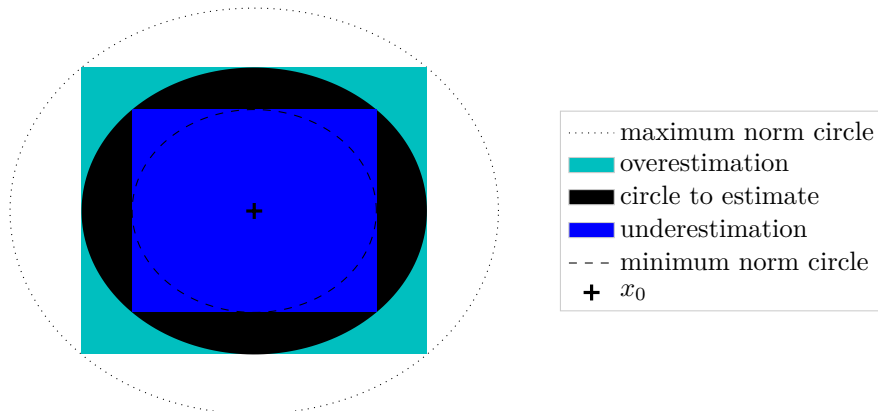


Figure 3: Bounding of a disk by (2) and (5) for $p = 4$ scalar products

the ratio of radius of cyan and black circles and the ratio of radius of black and blue circles minus one.

It turns out that the approximation error associated to (2) and (5) are both $\frac{1}{\cos \frac{\pi}{p}} - 1$ because the intervals in which approximation errors occur are $[\Delta, \frac{\Delta}{\cos \frac{\pi}{p}}]$ and $[\Delta \cos \frac{\pi}{p}, \Delta]$ respectively. Remark that the approximation error tends to 0 when the number of scalar products p tends to infinity, thus the linearizing method of [Camino et al., 2019] is an approximation that can be as good as needed by choosing p big enough.

2.3 Minimality of the Number of Scalar Product Used in the Linearization Scheme

This subsection is dedicated to the proof of theorem 2.3 that states that the linearizing scheme of [Camino et al., 2019] needs the minimum number of scalar products to satisfy a given euclidean norm approximation error threshold ϵ_0 as defined in definition 2.2. It creates a piecewise linear bounding for a given approximation error threshold that uses the minimal number of pieces. More precisely, what is proved is the following:

Let $\epsilon_0 > 0$ be the approximation error threshold to be satisfied for the approximation of a disk \mathcal{D} by a polygon. Let $p \in \mathbb{N}$ be such that

$$p = \min\{k \in \mathbb{N}^* : \frac{1}{\cos \frac{\pi}{k}} - 1 \leq \epsilon_0, k > 2\}$$

then a polygon contained in (resp. containing) the disk \mathcal{D} satisfying the approximation error threshold ϵ_0 has at least p sides, and the inner approximation (resp. outer approximation) of the disk with p scalar products given by the linearizing scheme of [Camino et al., 2019] produces a polygon with p sides satisfying the approximation error threshold.

Notation 1. Let \mathcal{P} be a polygon inside a disk \mathcal{D} centered at $(0,0)$. $\epsilon(\mathcal{P})$ denote the approximation error of the disk \mathcal{D} by the polygon \mathcal{P} according to definition 2.2.

The proof of theorem 2.3 treats separately the outer approximation and the inner approximation. The inner approximation case is dealt entirely before a justification that the proof scheme is similar for the outer approximation case is given.

The proof for the inner approximation case will be carried out through the following steps:

1. The number of sides of a non-convex polygon \mathcal{P} is strictly greater than the number of sides of its convex envelope $\text{conv}(\mathcal{P})$ and $\epsilon(\mathcal{P}) \geq \epsilon(\text{conv}(\mathcal{P}))$
2. given a number of sides p , a polygon of p sides satisfying the minimal approximation error is given by the inner approximation of a disk by p scalar products
3. the minimal approximation error decreases with the number of sides p of the polygons
4. conclusion of the proof of the theorem

For the sake of clarity, part 1 of the proof is stated as a lemma. Let \mathcal{D} be the unit disk. Let $\mathcal{P} \subset \mathcal{D}$ be a simple nonconvex polygon, where simple means that no edges of \mathcal{P} intersect except in the extreme points. Let $\mathcal{P}' = \text{conv}(\mathcal{P})$ be the convex envelope of \mathcal{P} . Then, $\mathcal{P}' \subset \mathcal{D}$, \mathcal{P}' has strictly less sides than \mathcal{P} and $\epsilon(\mathcal{P}) \geq \epsilon(\mathcal{P}')$. *Proof* First, $\mathcal{P} \subset \mathcal{D}$ implies that $\mathcal{P}' \subset \mathcal{D}$ because \mathcal{D} is convex. Second, a polygon is convex is equivalent to every angles of the polygon are lower than π . Now as \mathcal{P} is not convex, its convex envelope \mathcal{P}' has strictly less sides because at least one vertex of \mathcal{P} has an angle strictly greater than π and thus will not be a vertex of \mathcal{P}' . Third, $\mathcal{P} \subset \mathcal{P}' = \text{conv}(\mathcal{P})$ implies that the set over which is calculated the minimum a^- needed for the calculation of the approximation error in definition 2.2 is smaller for \mathcal{P}' than for \mathcal{P} , thus leading to $\epsilon(\mathcal{P}) \geq \epsilon(\text{conv}(\mathcal{P}))$. \square

According to the lemma, a polygon with the minimal number of sides to satisfy the approximation error threshold should be convex.

For part 2 of the proof let \mathcal{A}_p^- be the set of convex polygons of p sides lying inside \mathcal{D} the unit disk centered at $(0,0)$. The minus symbol refers to the inner approximation case:

$$\mathcal{A}_p^- = \{\mathcal{P} : \mathcal{P} \subset \mathcal{D} \text{ and } \mathcal{P} \text{ is a convex polygon with } p \text{ sides}\}$$

The unit disk is centered at $(0,0)$ because the number of sides of a polygon is invariant by homothetic transformation so it is always possible to return to this case from any disk centered at $x_0 \in \mathbb{R}^2$. Showing that the regular polygon with p sides on the circle is a solution of (9) is enough to prove part 2 of the proof.

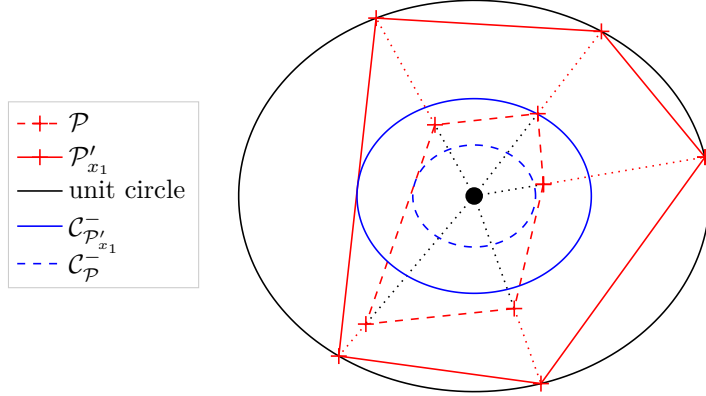


Figure 4: Inflation of \mathcal{P} by $x_1 = (0,0)$

$$(\mathcal{P}_p^-) \quad \begin{cases} \min & \epsilon(\mathcal{P}) \\ \text{s.c.} & \mathcal{P} \in \mathcal{A}_p^- \end{cases} \quad (9)$$

A definition of a specific transformation of a polygon is needed to show that this regular polygon of p sides is a solution of (9).

[inflation] Let $\mathcal{P} \in \mathcal{A}_p^-$ and let $x \in \text{Int}(\mathcal{P}) = \{x \in \mathcal{P} \setminus \text{Fr}(\mathcal{P})\}$ the interior of \mathcal{P} . Let "inflation of \mathcal{P} by x " denote the polygon \mathcal{P}'_x with vertices $v \in V$ obtained by intersection of the unit disk and the ray with initial point x and direction \vec{xw} with w a vertex of \mathcal{P} .

The two figures (4) and (5) illustrate this definition. They show the same dashed red polygon \mathcal{P} inflated by two different x , with circles showing the minimal norm of the polygons \mathcal{P} and \mathcal{P}'_x : in the first figure $x_1 = (0,0)$, and in the second $x_2 = (-0.25, -0.5)$. The inflated polygons \mathcal{P}' are in red, with dotted red lines showing the movement of the vertices. Finally, the dashed and solid blue circles are centered at $(0,0)$. They have for radius a^- of definition 2.2 for the approximation of \mathcal{B}_Δ the unit disk centered at $(0,0)$, respectively for \mathcal{P} and \mathcal{P}' .

Let \mathcal{P}'_x be the inflation of \mathcal{P} by $x \in \text{Int}(\mathcal{P})$. Then:

1. \mathcal{P}'_x is a polygon
2. $\text{Int}(\mathcal{P}) \subset \text{Int}(\mathcal{P}'_x)$
3. The vertices of \mathcal{P}'_x are on the circle
4. \mathcal{P}'_x is convex
5. \mathcal{P}'_x has the same number of sides as \mathcal{P}
6. $\epsilon(\mathcal{P}'_x) \leq \epsilon(\mathcal{P})$

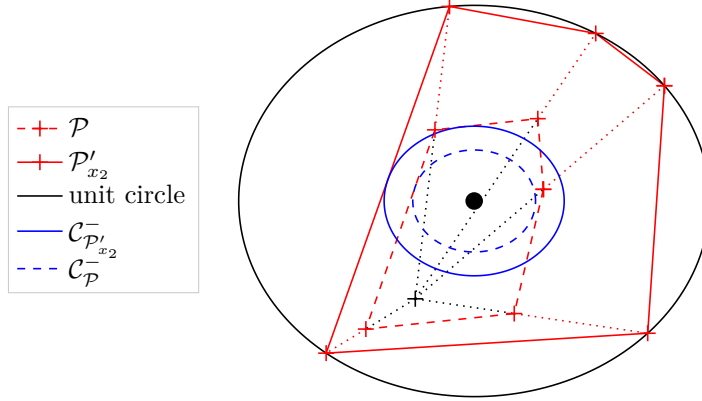


Figure 5: Inflation of \mathcal{P} by $x_2 = (-0.25, -0.5)$

Proof 1. \mathcal{P}'_x is a polygon if its frontier is a closed polygonal chain without intersections. As the vertices of \mathcal{P}'_x come from vertices of \mathcal{P} , by adding the straight line segments induced by the straight line segments of \mathcal{P} , \mathcal{P}'_x must be in a closed polygonal chain. To prove that there are no intersections in this polygonal chain, remark that the p rays used to build the inflation are intersecting in x , and that an intersection of the polygonal chain of \mathcal{P}'_x would mean that two of those rays intersect in another point meaning that the two rays overlap, which is impossible because \mathcal{P} is convex and $x \in \text{Int}(\mathcal{P})$.

2. \mathcal{P} can be decomposed into p triangles in the following way: each triangle has for vertices x , and two vertices of \mathcal{P} connected by an edge. Decompose \mathcal{P}'_x in the same way. Each triangle T of \mathcal{P} is included in one triangle T' of \mathcal{P}'_x : the one for which the two vertices of T moved to the two vertices of T' with the inflation. The inclusion stands because those two vertices have been moved along the sides of triangle T in the opposite direction of the third vertex x .

3. By definition of inflation.

4. A polygon with all vertices on the unit circle and with no self intersection as seen in the proof of part 1 is convex because the angle of every vertex with its two neighbours is strictly less than π .

5. \mathcal{P}'_x has no more than p vertices by definition. Suppose by contradiction that \mathcal{P}'_x has at least one vertex less than \mathcal{P} . Thus, there exists a vertex v' of \mathcal{P}'_x that has been obtained by two different vertices v_1 and v_2 of \mathcal{P} . It means that those two vertices lies in the same ray with initial point x . Thus, say v_1 is a linear combination of x and v_2 , which contradicts it being an extreme point because \mathcal{P} is convex.

6. By 2, it is known that $\mathcal{D} \setminus \text{Int}(\mathcal{P}') \subset \mathcal{D} \setminus \text{Int}(\mathcal{P})$, thus $\min\{\|x\|_2 : x \in \mathcal{D} \setminus \text{Int}(\mathcal{P}')\} \geq \min\{\|x\|_2 : x \in \mathcal{D} \setminus \text{Int}(\mathcal{P})\}$, leading to 6. \square

Point 6 of proposition 2.3 gives that there is a polygon with each vertex on the circle that is solution of (9). Thus the focus is on the analysis of such

polygons. The approximation error is calculated with the point of minimal norm of $\mathcal{D} \setminus \text{Int}(\mathcal{P})$. The following proposition states which point of $\mathcal{D} \setminus \text{Int}(\mathcal{P})$ is this minimal norm point.

Let $\mathcal{P} \in \mathcal{A}_P^-$ be a polygon with vertices on the circle. If $(0, 0) \in \text{Int}(\mathcal{P})$, then the minimal norm point $x \in \mathcal{D} \setminus \text{Int}(\mathcal{P})$ is $\|\overrightarrow{OD}\|_2$ where D is the middle point of the longest side of \mathcal{P} .

Proof It is obvious that the minimal norm point is on a side of \mathcal{P} because $(0, 0) \in \text{Int}(\mathcal{P})$.

Every side of the polygon \mathcal{P} has endpoints of norm one, and a computation shows that the minimal norm point of a side with this property is its middle point M . Moreover, by considering the triangle decomposition of a polygon like in proof of point 2 of proposition 2.3 with additional point the origin $(0, 0)$, it is possible to compute the norm of M with the angle α of the triangle at point $(0, 0)$. The computation gives that its norm is $\cos \frac{\alpha}{2} =: g(\alpha)$. As $(0, 0) \in \text{Int}(\mathcal{P})$, $\alpha \in]0, \pi[$.

Finally, $g'(\alpha) < 0$ on $]0, \pi[$ so the norm of the middle point of a side of \mathcal{P} decreases when the angle α increases, which is equivalent to when the length of the side increases, leading to the result. \square

The hypothesis made for proposition 2.3 is not a limiting one because if the origin $(0, 0) \notin \text{Int}(\mathcal{P})$, the approximation error of \mathcal{P} is infinite whereas there always exists a polygon with a finite approximation error so it is not an optimal solution of (9).

This result shows that this is the longest side of a polygon with vertices on the circle that will determine the approximation error of the polygon. It leads to the following result:

The regular polygon of p sides with all vertices on the circle is an optimal solution of (9) and its objective value is $\frac{1}{\cos \frac{\pi}{p}} - 1$.

Proof Let $(\alpha_1, \dots, \alpha_p)$ be the angles at $(0, 0)$ associated to each of the p triangles of \mathcal{P} as in the last proof. A solution of (9) is a polygon with all vertices on the circle that is also solution of:

$$\min_{\mathcal{P} \in \mathcal{A}_P^-} \max_{i=1, \dots, p} \alpha_i \quad (10)$$

The only solution of (10) is $\alpha_i = \frac{2\pi}{p}$ $i = 1, \dots, p$. Thus the p triangles making the polygons have the same angle at $(0, 0)$ and thus they are all similar. Going back to the polygon, it means that every sides have the same length. As the polygon is equilateral and inscriptible in a circle, it is a regular polygon with p sides. Finally, the optimal value is $\frac{1}{\cos \frac{\pi}{p}} - 1$ by calculating the norm of the middle point of any of the side of the regular polygon of p sides with vertices on the circle. \square

It ends part 2 of the proof of theorem 2.3. For part 3, the result is once again in a lemma: The solution of (9) decreases with p .

Proof According to theorem 2.3, the optimal objective value of (9) is $\frac{1}{\cos \frac{\pi}{p}} - 1$, which decreases with p . \square

All the pieces of the proof of theorem 2.3 are put together in the following:

Proof[proof of theorem 2.3] Let $\epsilon_0 > 0$. Let \mathcal{D} be the unit disk centered at $(0, 0)$. Let $p = \min\{k \in \mathbb{N}^* : \frac{1}{\cos \frac{\pi}{k}} - 1 \leq \epsilon_0, k > 2\}$. Then theorem 2.3 and lemma 2.3 gives that a polygon satisfying the approximation error threshold ϵ_0 has at least p sides and a regular polygon with p sides satisfies the approximation error threshold ϵ_0 . As the inner approximation of a disk with p scalar products yields a regular polygon with p sides, it satisfies the approximation error threshold.

If \mathcal{D} was not the unit disk, an homothetic transformation would bring back \mathcal{D} to the unit disk and the same transformation applied to the polygon would not change its number of sides, so the result is valid for any disk.

Finally, the outer approximation case can be treated in the same manner. Indeed, part 1 is also true, with in bonus the equality $\epsilon(\mathcal{P}) = \epsilon(\text{conv}(\mathcal{P}))$. Part 2 is proved in a similar way, with two replacements:

- replace the inflation of definition 2.3 by a deflation: the sides of the polygon are moved in the direction of the center of the disk so as to keep them parallel to there initial position until they are tangent to the circle
- replace the angles α_i associated to each of the p triangles at point $(0, 0)$ in the proof of theorem 2.3 by angles directly on the vertices of the deflated polygon

Finally, part 3 and part 4 are proved in an analoguous way. □

3 Extensions of the Euclidean Norm Linearization

In this section, two extensions of the linearization of [Camino et al., 2019] are discussed. Moreover, the result of 2.3 is transposable to the extensions. The first is the linearization of the euclidean norm of \mathbb{R}^2 directly in the objective function. An optimal polyhedron in terms of number of pieces for a given error ϵ is constructed. This result is based on the absolutely homogeneous property of a norm. The second extension concerns constraints, and is valid with a class of norms of elliptic level set. This result comes from the fact that an ellipse is a linear deformation of a circle, so that an optimal polygon overestimating a disk with a given error gives an optimal polygon overestimating an ellipse simply by applying the linear deformation that transforms the circle into the ellipse.

3.1 Linearization in the Objective Function

The euclidean norm linearization can be used to linearize the euclidean norm of \mathbb{R}^2 in a constraint, but also in the objective function as shown in this subsection. After introducing the parametric equation of a positive cone, the construction of the optimal piecewise linear bounding of the euclidean norm of \mathbb{R}^2 for a given error is shown.

The surface generated by the euclidean norm of \mathbb{R}^2 is the positive cone \mathcal{C} (11).

$$\begin{aligned}\mathcal{C} &= \{(x_1, x_2, x_3) : x_3 = \|(x_1, x_2)\|_2, x_1 \in \mathbb{R}, x_2 \in \mathbb{R}\} \\ &= \{(x_1, x_2, x_3) \in \mathbb{R}^3 : x_1^2 + x_2^2 - x_3^2 = 0 \text{ and } x_3 \geq 0\}\end{aligned}\quad (11)$$

Before introducing the bounding of the positive cone, recall the definition of equally spaced unit vectors for the linearization, with an integer $p > 2$,

$$\mathbf{u}_i = \left(\cos \frac{2i\pi}{p}, \sin \frac{2i\pi}{p}\right) \text{ for } i = 1, \dots, p$$

and let \mathcal{C}_p^+ and \mathcal{C}_p^- be defined as in (12) and (13),

$$\mathcal{C}_p^+ = \{(x_1, x_2, f_p^+(x_1, x_2)) : x = (x_1, x_2) \in \mathbb{R}^2\} \quad (12)$$

$$\mathcal{C}_p^- = \{(x_1, x_2, f_p^-(x_1, x_2)) : x = (x_1, x_2) \in \mathbb{R}^2\} \quad (13)$$

with $f_p^+(x_1, x_2)$ and $f_p^-(x_1, x_2)$ equal to:

$$f_p^+(x_1, x_2) = \max_{i=1, \dots, p} \frac{(x_1, x_2)^T \cdot \mathbf{u}_i}{\cos \frac{\pi}{p}} \quad (14)$$

$$f_p^-(x_1, x_2) = \max_{i=1, \dots, p} (x_1, x_2)^T \cdot \mathbf{u}_i \quad (15)$$

The surface induced by the inner approximation of p scalar products is denoted \mathcal{C}_p^+ because it is an *overestimation* of \mathcal{C} in the sense that given $(x_1, x_2) \in \mathbb{R}^2$, x_3 such that $(x_1, x_2, x_3) \in \mathcal{C}$ and x_3^+ such that $(x_1, x_2, x_3^+) \in \mathcal{C}_p^+$, then $x_3 \leq x_3^+$.

Similarly, the surface induced by the outer approximation of p scalar products is an *underestimation* of \mathcal{C} and is denoted \mathcal{C}_p^- .

The terms underestimation, overestimation and bounding for functions are defined more precisely below.

Let $f, f^-, f^+ : \mathbb{R}^2 \rightarrow \mathbb{R}^+$. $F_0 := \{x \in \mathbb{R}^2 : f(x) = 0\}$ is the level set of 0 of f . Let $F_0^- := \{x \in \mathbb{R}^2 : f^-(x) = 0\}$. Then there exists $\epsilon > 0$ such that for all $x \in \mathbb{R}^2 \setminus F_0$

$$\frac{f(x) - f^-(x)}{f^-(x)} \in [0, \epsilon] \quad (16)$$

It is denoted f is *underestimated* by f^- with approximation error ϵ . If $f^+(x) = 0$ on F_0 and there exists $\epsilon > 0$ such that for all $x \in \mathbb{R}^2 \setminus F_0$

$$\frac{f^+(x) - f(x)}{f(x)} \in [0, \epsilon] \quad (17)$$

It is denoted f is *overestimated* by f^+ with approximation error ϵ .

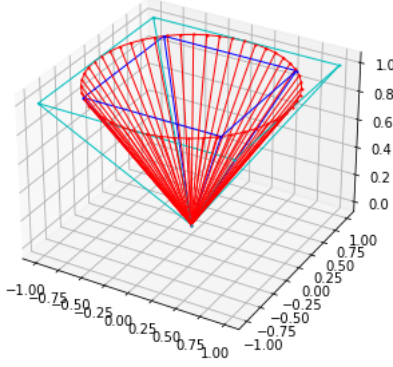


Figure 6: Linear bounding of the positive cone seen from above for $P = 4$ scalar products

If f^- , f^+ are such that $f^-(x) = f^+(x) = 0$ on F_0 and there exists $\epsilon > 0$ such that both (16) and (17) are satisfied, then it is denoted f is bounded by f^- and f^+ with approximation error ϵ . If in addition f^- and f^+ are piecewise linear functions, it is referred as a *linear bounding*.

In figure 6, a 3D representation of \mathcal{C} in red, \mathcal{C}_p^- in cyan and \mathcal{C}_p^+ in blue is shown.

Let $p \in \mathbb{N}$, $p > 2$. $\|x\|_2$ is linearly bounded by f_p^- and f_p^+ with approximation error $\frac{1}{\cos \frac{\pi}{p}} - 1$.

Proof The proof that f is overestimated by f_p^+ with approximation error $\frac{1}{\cos \frac{\pi}{p}} - 1$ is given here. The inner approximation case is similar.

Proving (18) is sufficient since it is equivalent to (17) for $f^+(x) = f_p^+(x)$, $f(x) = \|x\|_2$ and $\epsilon = \frac{1}{\cos \frac{\pi}{p}} - 1$.

$$\frac{f_p^+(x)}{\|x\|_2} \in [1, \frac{1}{\cos \frac{\pi}{p}}] \quad \forall x \in \mathbb{R}^2 \quad (18)$$

Remark that \mathcal{C}_p^+ is stable by a $\frac{2\pi}{p}$ angle rotation around axis x_3 because the regular polygon with p sides used to construct \mathcal{C}_p^+ has this property. Thus proving (18) for $x \in X_p = \{(\alpha \cos \beta, \alpha \sin \beta) : \alpha \geq 0, \beta \in [-\frac{\pi}{p}, \frac{\pi}{p}]\}$ is sufficient because $Z_p^+ := \{(x_1, x_2, f_p^+(x_1, x_2)) : (x_1, x_2) \in X_p\}$ is the set of points on one face of the outer approximation \mathcal{C}_p^+ . Moreover, (19) is a parametrisation of the face Z_p^+ .

$$Z_p^+ = \{(\alpha_+ \cos \frac{\pi}{p}, \beta_+, \alpha_+) : \alpha_+ \geq 0, \beta_+ \in [-\alpha_+ \sin \frac{\pi}{p}, \alpha_+ \sin \frac{\pi}{p}]\} \quad (19)$$

Vectors of Z_p^+ can all be written uniquely as $\alpha_+ u + \beta_+ v$ with $\alpha_+ > 0$ and $\beta_+ \in [-\alpha_+ \sin \frac{\pi}{p}, \alpha_+ \sin \frac{\pi}{p}]$. (20) is a parametrisation of Z_p which is the piece of

\mathcal{C} estimated by Z_p^+ .

$$Z_p := \{(\alpha \cos \beta, \alpha \sin \beta, \alpha) : \alpha \geq 0, \beta \in [-\frac{\pi}{p}, \frac{\pi}{p}]\} \quad (20)$$

Let $x \in X_p$. We will show that $1 \leq \frac{f_p^+(x)}{\|x\|_2} \leq \frac{1}{\cos \frac{\pi}{p}}$. Let $\alpha \geq 0$ and $\beta \in [-\frac{\pi}{p}, \frac{\pi}{p}]$ so that $x = (\alpha \cos \beta, \alpha \sin \beta)$. It is known that $f(x) = \alpha$. To find the point $(\alpha_+ \cos \frac{\pi}{p}, \beta_+, \alpha_+)$ of Z_p^+ , it suffices to solve (21).

$$\begin{cases} \alpha \cos \beta = \alpha_+ \cos \frac{\pi}{p} \\ \alpha \sin \beta = \beta_+ \end{cases} \quad (21)$$

The solution is (22).

$$\begin{cases} \alpha_+ = \alpha \frac{\cos \beta}{\cos \frac{\pi}{p}} \\ \beta_+ = \alpha \sin \beta \end{cases} \quad (22)$$

Thus:

$$\frac{f^+(x)}{\|x\|_2} = \frac{\cos \beta}{\cos \frac{\pi}{p}} \in [1, \frac{1}{\cos \frac{\pi}{p}}] \quad \forall \beta \in [-\frac{\pi}{p}, \frac{\pi}{p}] \quad (23)$$

And the upper bound of the interval $[1, \frac{1}{\cos \frac{\pi}{p}}]$ is reached for $\beta = 0$. Thus $\epsilon = \frac{1}{\cos \frac{\pi}{p}}$ is the approximation error. \square

Let the required approximation error be $\epsilon \in [\frac{1}{\cos \frac{\pi}{p}}, \frac{1}{\cos \frac{\pi}{p-1}}[$, with $p \in \mathbb{N}$, $p > 2$. Then the linear bounding of the euclidean norm by f_p^- and f_p^+ uses the minimum number of pieces.

Proof The number of sides of the polygon induced by the euclidean norm linearization for a constraint is optimal. Moreover, the linear bounding of the euclidean norm uses the same number of pieces for the same approximation error. As this linear bounding is constructed upon the polygon, it gives a lower bound of the number of pieces for the linear bounding, lower bound that is reached. \square

Thus the euclidean norm linearization of [Camino et al., 2019] can be used to derive a linear bounding which uses the minimum number of pieces for two piecewise linear functions to bound the euclidean norm of \mathbb{R}^2 .

3.2 Extension to Elliptic Constraints

As mentionned previously, it is possible to adapt the linearization of [Camino et al., 2019] for norms with elliptic level sets in constraints. Such constraints are denoted *elliptic constraints*. A gathering of useful definitions on ellipses is followed by the construction of the linear bounding of elliptic constraints using the minimal number of pieces.

Recall that an ellipse \mathcal{E} with center (u, v) , width a , height b (i.e. with no angle between the horizontal axis and the major axis) is a subset of \mathbb{R}^2 such that:

$$\frac{(x-u)^2}{a^2} + \frac{(y-v)^2}{b^2} = 1 \quad \forall (x, y) \in \mathbb{R}^2 \quad (24)$$

by adding an angle θ , width and height are replaced by semi-major axis a and semi-minor axis b :

$$\frac{((x-u)\cos\theta - (y-v)\sin\theta)^2}{a^2} + \frac{((x-u)\sin\theta + (y-v)\cos\theta)^2}{b^2} = 1 \quad \forall (x, y) \in \mathbb{R}^2 \quad (25)$$

In this subsection, the previous results on the approximation error of the euclidean norm linearization are extended to norms with ellipses as level sets. Such a norm is denoted $\|\cdot\|_{a,b,\theta}$, and its definition is written:

$$\|x\|_{a,b,\theta}^2 = \frac{((x_1 \cos\theta - x_2 \sin\theta)^2}{a^2} + \frac{((x_1 \sin\theta + x_2 \cos\theta)^2}{b^2} \quad \forall x = (x_1, x_2) \in \mathbb{R}^2, a, b \in \mathbb{R}_*^+ \quad (26)$$

The vocabulary used for ellipses is defined below:

- the shape of an ellipse is denoted (a, b) where a and b are the semi-major axis and semi-minor axis respectively (which means $a \geq b > 0$).
- the angle of an ellipse θ refer to the angle between the horizontal axis and the major axis, with $\theta \in [-\frac{\pi}{2}, \frac{\pi}{2}]$.

Remark that any non-degenerate ellipse can be obtained by a linear transformation of a circle: a circle is a specific ellipse with $a = b = R$ and $\theta = 0$ with R the radius of the circle. This linear transformation is a change of basis to an orthogonal basis followed by a translation. Without the translation, ϕ is the linear transformation from a circle of radius 1 centered at the origin and an ellipse of shape (a, b) , angle θ and centered at the origin:

$$\phi_{a,b,\theta} : \mathbb{R}^2 \rightarrow \mathbb{R}^2 \quad (27)$$

$$(x, y) \mapsto (ax \cos\theta - by \sin\theta, ax \sin\theta + by \cos\theta) \quad (28)$$

As this transformation is linear with the inverse transformation $\phi_{a,b,\theta}^{-1}$ is also linear (see figure 7) and it preserves the norm ratio between two colinear vectors. Thus, the regular polygon with p sides obtained by the euclidean norm linearization is, after transformation by $\phi_{a,b,\theta}$, a polygon that uses the minimum number of sides to satisfy a given approximation error for the ellipse of shape (a, b) and angle θ .

This analysis shows that constraints involving elliptic norms can also be linearized by the euclidean norm linearization, after a suitable change of basis

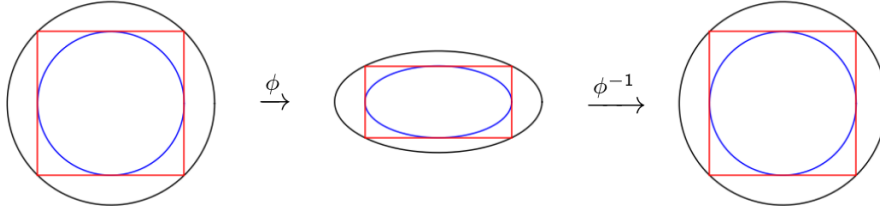


Figure 7: Linear transformation between a circle and an ellipse

(as well as linearization of ellipses in the objective function). A procedure to linearize a constraint $\|x\|_{a,b,\theta} \leq \Delta$ is thus to replace it by (29).

$$\|\phi_{a,b,\theta}^{-1}(x)\|_{a,b,\theta} \cdot \mathbf{u}_i \leq d\Delta \quad \forall i = 1, \dots, p \quad (29)$$

with $d = \frac{1}{\cos \frac{\pi}{p}}$ for an inner approximation and $d = 1$ for an outer approximation.

A downside of this linearization is that a , b and θ have to be constants of the model or it would induce nonlinear terms. It means that to linearize a constraint "x is in an ellipse" with the ellipse's shape and angle not fixed, a discretization of the possible ellipses parameters that yields many constraints is needed: with n tuples (a, b, θ) and p scalar products, it is necessary to use np big-M constraints instead of p for the circle to achieve the same approximation error. Thus, the model is not suited for really fine discretization of possible ellipses.

However, the next section presents an application for which the proposed linearization is useful.

4 Application to the Beam Layout Problem

The interest of the extension of the euclidean norm linearization is demonstrated on a mixed continuous/discrete optimisation problem with elliptic constraints. The considered problem is derived from a beam layout problem arising in satellite telecommunications. The original problem has been tackled in [Camino et al., 2014, 2016, 2019, 2021] and does not involve elliptic constraints. We refer to [Camino et al., 2021] for a state-of-the-art review on this problem. Informally, a satellite equipped with a multibeam antenna has to cover a set of end users inside a predefined area on earth by means of a set of movable beams (see Figure 8). In the original problem the projected surface of the beam is circular. Hence, a user is covered if its coordinates are inside one of the beam disks, i.e. if a proximity constraint between the user and the beam center is satisfied. There are also separation constraints between the beam centers depending on discrete beam/reflector assignment constraints as explained in details below. However, in modern multibeam antennas systems the beam shape need not be circular as reconfigurable antennas allow to obtain different beam shapes including elliptic

ones [Rao et al., 2006]. Adding the possibility of elliptic beam shape in addition to circular ones obviously increases the covering power of the system by a better potential adaptation to the area containing the end users. However, the complexity of proximity and separation constraint modeling is increased, due to the extra constraints required for linearization of ellipses as explained above. The aim of the experimental study carried out in this section is to determine if this complexity increase is compensated by the gain in the objective function for a limited amount of CPU time compared to the model allowing only circular beams.

The first subsection explains the modeling of the beam layout problem, while the second provides the numerical results.

4.1 Problem Definition and Formulation

A multibeam satellite is a telecommunication satellite that uses relatively narrow beams to provide a service to users on earth. It has different reflector antennas and each beam is associated to a reflector antenna.

In the considered beam layout problem, a multibeam satellite provides services via beams $b \in B$, each produced by a reflector $r \in R$. On earth, user stations $s \in S$ of coordinates (X_s, Y_s) are characterised by their traffic demand $T_s \in \mathbb{R}^+$. They can be covered by a beam of the multibeam satellite. A station s is considered covered by the satellite if at least one beam b covers the station. Each beam covers a portion of the earth in the shape of an ellipse of predefined parameters. The goal is to maximise the traffic covered while satisfying a maximum capacity of covering by a beam and some separation constraints coming from technology constraints: each beam of the satellite is associated to a reflector and two beams of the same reflector cannot be too close from each other as explained in [Camino et al., 2014]. It forces two beams of the same reflector enlarged by a factor κ to not intersect. Beams used in [Camino et al., 2019] covers a circular region on earth, but, as mentioned above, it is technically possible to use beams of elliptic shapes.

Each beam can be an ellipse of shape $(a_k, \frac{1}{a_k})$, $a_k \geq 1$ with $k \in K$ given, and angle $\theta \in \Theta$ given. This choice of shape ensures that every ellipse covers the same surface on earth, thus no ellipse's shape is advantaged over another. A model of the beam layout problem is given in (30)-(41).

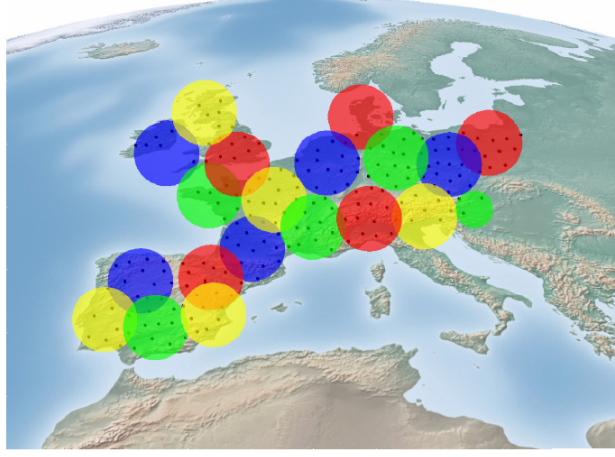


Figure 8: Example of beam layout solution with only circles as beam shape

$$\text{Max} \sum_{(b,s) \in B \times S} T_s \alpha_{s,b} \quad (30)$$

$$\text{s.t.} \sum_{b \in B} \alpha_{s,b} \leq 1 \quad \forall s \in S \quad (31)$$

$$\sum_{r \in R} \beta_{b,r} \leq 1 \quad \forall b \in B \quad (32)$$

$$\sum_{s \in S} T_s \alpha_{s,b} \leq \gamma \quad \forall b \in B \quad (33)$$

$$\sum_{k \in K, \theta \in \Theta} \delta_{b,k,\theta} = 1 \quad \forall b \in B \quad (34)$$

$$\|(x_b, y_b) - (X_s, Y_s)\|_{a_k, \frac{1}{a_k}, \theta} \leq W + (2 - \alpha_{s,b} - \delta_{b,k,\theta}) M_s \quad \forall s \in S, \forall b \in B, \forall k \in K, \forall \theta \in \Theta \quad (35)$$

$$\gamma_{b,b'} \geq \sum_{r' \in R} \beta_{b,r'} + \sum_{r' \in R} \beta_{b',r'} + \beta_{b,r} + \beta_{b',r} - 3 \quad \forall b, b' \in B, b' > b, \forall r \in R \quad (36)$$

$$\|(x_b, y_b) - (x_{b'}, y_{b'})\|_{a_k, \frac{1}{a_k}, \theta} \geq 2\kappa W - N(1 - \gamma_{b,b'}) \quad \forall b, b' \in B, b' \neq b \quad (37)$$

$$x_b, y_b \geq 0 \quad \forall b \in B \quad (38)$$

$$\alpha_{s,b} \in \{0, 1\} \quad \forall s \in S, \forall b \in B \quad (39)$$

$$\beta_{b,r} \in \{0, 1\} \quad \forall b \in B, \forall r \in R \quad (40)$$

$$\delta_{b,k,\theta} \in \{0, 1\} \quad \forall b \in B, \forall k \in K, \forall \theta \in \Theta \quad (41)$$

(30) is the maximisation of the covered traffic, with $\alpha_{s,b}$ a binary variable equal to 1 if user station s is covered by beam b . Constraint (31) forces a station to be covered by at most one beam. Constraint (32) associates a reflector antenna r to each beam b due to the binary variable $\beta_{b,r}$. Constraint (33) ensures that each beam cannot cover more than a traffic of γ . Constraint (34) associates a shape $(a_k, \frac{1}{a_k})$ and an angle $\theta \in \Theta$ to a beam b through the use of the binary variable $\delta_{b,k,\theta}$. Constraint (35) checks that each station s is in the beam b of center (x_b, y_b) to which it is affected, with M_s the big-M constant associated and $\|\cdot\|_{a_k, \frac{1}{a_k}, \theta}$ the norm defined in (26) with level set for the value 1 the ellipse of shape $(a_k, \frac{1}{a_k})$ and angle θ . Constraint (36) enforces that the binary variable $\gamma_{b,b'}$ is equal to 1 if beams b and b' come from the same reflector antenna. Constraint (37) ensures that two beams associated to the same reflector antenna b and b' are not too close. Finally, (38)-(41) define variable types.

The details of the linearization into an MILP model are discussed here. The nonlinearity comes from constraints (35) and (37). As explained in (29), the linearization procedure is to apply a suitable linear transformation and then apply the euclidean norm linearization. Moreover, constraint (36) needs to be adapted to the linearization. Thus, the only constraints that change in the linearization are (35), (36) and (37).

Let p be the number of scalar product used to linearize, according to an error approximation ϵ wanted. Let $\phi_{a_k, \frac{1}{a_k}, \theta}^{-1}$ be the linear transformation defined in (29). For $i = 1, \dots, p$, the linearization of (35) is (42). The right part contains $\cos \frac{\pi}{p}$ to ensure feasibility, which corresponds to the inner approximation of the disk.

$$\forall s \in S, \forall b \in B, \forall k \in K, \forall \theta \in \Theta, \forall i = 1, \dots, p :$$

$$\phi_{a_k, \frac{1}{a_k}, \theta} \left(\begin{pmatrix} x_b - X_s \\ y_b - Y_s \end{pmatrix} \right) \cdot \begin{pmatrix} \cos \frac{2\pi i}{p} \\ \sin \frac{2\pi i}{p} \end{pmatrix} \leq W \cos \frac{\pi}{p} + (2 - \alpha_{s,b} - \delta_{b,k,\theta}) M_s \quad (42)$$

Constraint (37) is not as easy to linearize. Indeed, this is not a convex constraint: it is about ensuring that two ellipses do not intersect. In the case of ensuring that two disks do not intersect (created by two beams of circle shape), it suffices to evaluate the distance between the two centers, that is to say apply the euclidean norm linearization and then ensure with big-M constraints that this distance is higher than what is necessary. For two ellipses, this linearization scheme does not work. The convexity of an ellipse allows to model the intersection with linear separation in a similar way as [Kallrath and Rebennack, 2014].

Let $A, B \subset \mathbb{R}^2$. A and B are linearly separated if

$$\exists v \in \mathbb{R}^2, \exists b \in \mathbb{R} : \forall x \in A, \forall y \in B : x.v \leq b \leq y.v$$

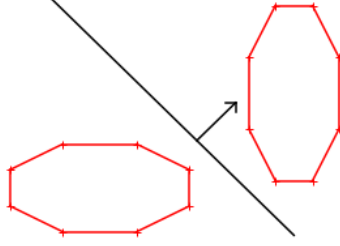


Figure 9: Linear separation of two ellipses outer approximations by the black line

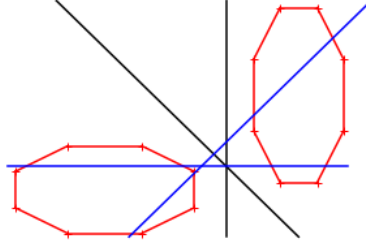


Figure 10: The linear separation is working with the two black lines and is not working with the two blue ones

The linear separation is illustrated in figure 9: the two octagons are linearly separated because a line d can be drawn between them, which corresponds to the hyperplane $d = \{u \in \mathbb{R}^2 : u.v = b\}$. The ellipses approximations are convex polygons so it suffices to test the linear separation with the vertices of those polygons. The last problem for the linearization is that making scalar products between variable vectors is a quadratic operation. To adress this issue, the linear separation is tested only for a finite number N_{dir} of hyperplanes of normal vectors $v_j = (\cos \frac{2j\pi}{p}, \sin \frac{2j\pi}{p})$ for $j = 1, \dots, N_{dir}$. This means that a stronger version of the linear separation is ensured in the model, but with a reasonably high value for N_{dir} , it is probably good enough compared to the other approximations of the model.

Constraint (36) becomes (43)-(44). The new binary variables $\gamma_{b,b',j}$ replace $\gamma_{b,b'}$ because for the linearization, selecting which line j is associated to v_j for $j = 1, \dots, N_{dir}$ ensures the linear separation.

$$\sum_{j=1}^{N_{dir}} \gamma_{b,b',j} \geq \sum_{r \in R} \beta_{b,r} + \sum_{r \in R} \beta_{b',r} + \beta_{b,r} + \beta_{b',r} - 3 \quad (43)$$

$$\forall r \in R, \forall b, b' \in B \text{ such that } b' > b \quad (44)$$

Finally the linearization of (37) becomes (45)-(47). $(S_i^{x,b}, S_i^{y,b})$ are the co-

ordinates of the vertex i of outer approximation of beam b . The outer approximation of the disk is used to ensure feasibility. N is the big-M constant of the constraint.

$$\begin{pmatrix} S_i^{x,b} \\ S_i^{y,b} \end{pmatrix} \cdot \begin{pmatrix} \cos \frac{2\pi k}{N_{dir}} \\ \sin \frac{2\pi k}{N_{dir}} \end{pmatrix} \leq w_{b,b'} + N(1 - \gamma_{b,b',k}) \quad (45)$$

$$\begin{pmatrix} S_i^{x,b'} \\ S_i^{y,b'} \end{pmatrix} \cdot \begin{pmatrix} \cos \frac{2\pi k}{N_{dir}} \\ \sin \frac{2\pi k}{N_{dir}} \end{pmatrix} \geq w_{b,b'} + N(1 - \gamma_{b,b',k}) \quad (46)$$

$$\forall b, b' \in B \text{ such that } b' \neq b, \forall i = 1, \dots, P, \forall k = 1, \dots, N_{dir} \quad (47)$$

4.2 Computational Experiments

In this part, the goal is to evaluate the potential of the extension of the euclidean norm linearization to ellipses. Thus, a comparison of the euclidean norm linearization (CL for Circle Linearization) to its extension to ellipses (EL for Ellipse Linearization) is done on the beam layout problem. Beams of elliptic shapes are used for model EL, while only circles are used for model CL.

A set of 100 instances is considered, corresponding to different sizes, different number of scalar products p used in the linearizations and different densities. As for sizes, there are five different sizes : the number of stations $|S|$ vary in $\{20, 40, 60, 80, 100\}$ with associated number of beams $|B| = \min\{\frac{|S|}{8}, 10\}$ which is $|B| \in \{3, 5, 7, 10\}$. As for p , it was taken from the set $\{4, 8, 12, 16, 20\}$. Concerning densities, two different values $d \in \{30, 70\}$ are used. Thus there are 10 different instances for each couple (size, density). For each instance, the stations positions are drawn randomly from a set of 157 positions from a real instance and there are three reflector antennas. Each of those 100 instances have been solved by the two different models, CL and EL, for three different maximum computation times which are 600, 1800 and 3600 seconds. The ellipses allowed in the EL model are $\phi_{a, \frac{1}{a}, \theta}$ with $a \in A = \{\frac{1}{2}, 1, 2\}$ and $\theta \in \Theta = \{\frac{2\pi}{3}, \frac{4\pi}{3}, 1\}$. Each ellipse allowed is visible on figure 11. Moreover, the capacity γ is fixed to 500 in all instances. It is a major limitation for the objective value as the naive upper bound induced by the capacity is pretty close to the objective value in many instances. Examples of solutions are plotted in figure 12 and 13. Black points are not covered stations, colored points are covered stations, and the color indicate the reflector antenna which possesses the beam covering the station.

Due to the size of instances, the parameter N_{dir} has a really low impact on both time and objective function value, so for every instances it is set to 10.

Every instance is solved on one core of a Xeon E5-2695 v3 @ 2.30GHz CPU with a RAM limit of 3.5 Go. The solver used is CPLEX 12.9 with the global thread count parameter set to 1.

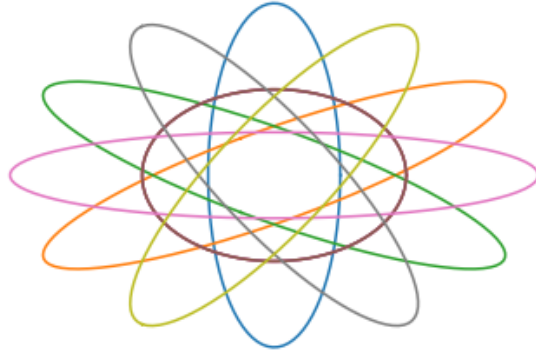


Figure 11: Beam shapes allowed for the instances solved with the EL linearization

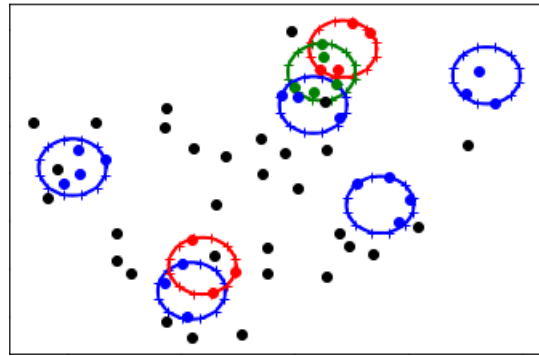


Figure 12: Example of feasible solution for the circle model

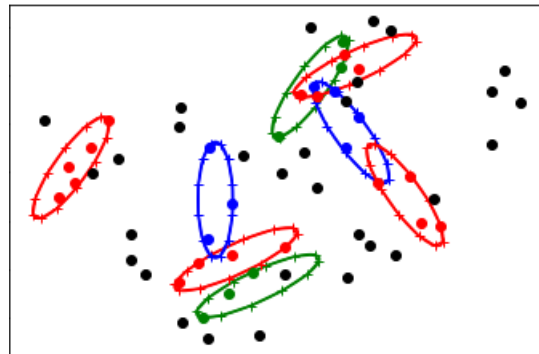


Figure 13: Example of feasible solution for the ellipse model

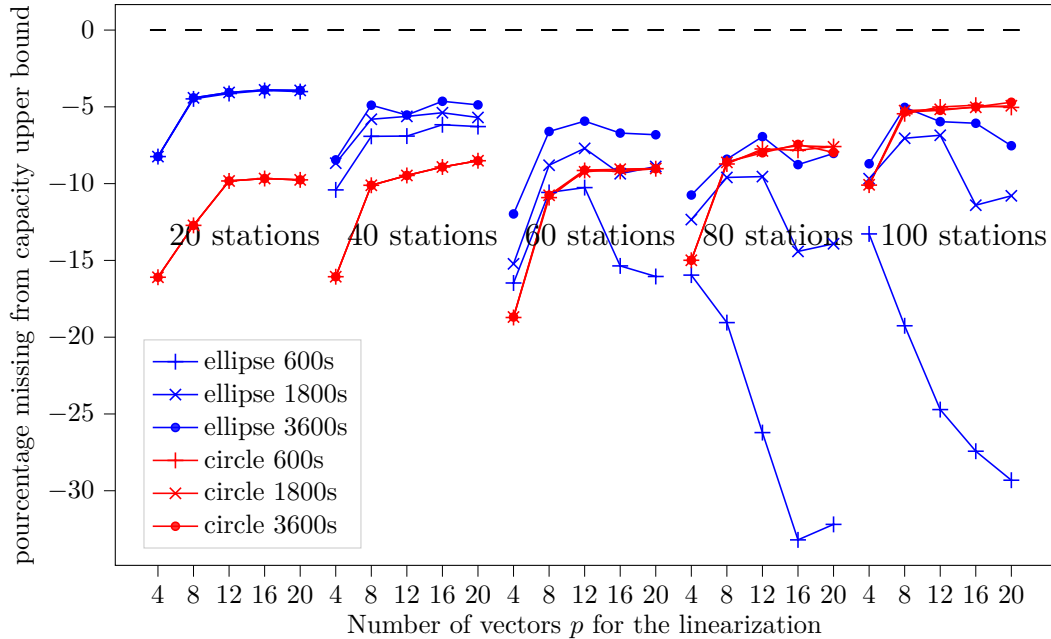


Figure 14: Results for low density instances

Figures 14 and 15 show the results for low and large densities, respectively. Each point represents a relative gap of a mean over 10 instances from a naive upper bound in percentage. The gap is calculated with formula $100 \frac{M - \gamma|B|}{M}$ with M the mean objective value and $\gamma|B|$ the naive upper bound derived from the maximum capacity $|S|$ beams can cover. This naive upper bound is plotted in the dashed black line. The points linked represents values obtained from instances with the same model, the same time limit and the same number of stations $|S|$, thus there are five different series of plots, representing the 5 different numbers of stations used.

There are few instances solved to optimality due to the big size of the model solved, and the EL model produces bigger models so less EL model instances are solved to optimality than CL model instances. There are only 12 % of all instances solved with the EL model that are solved to optimality, and all those instances are with 20 stations. As for instances solved with CL model, 35 % are solved to optimality, with all 20 stations instances, and 73 % of 40 stations instances. None of the others are solved to optimality. Thus, the following comparison should only be taken as a practical comparison and not as a comparison of optimal value since most of the instances are not solved to optimality.

There are some visible facts on figures 14 and 15. For a high number of

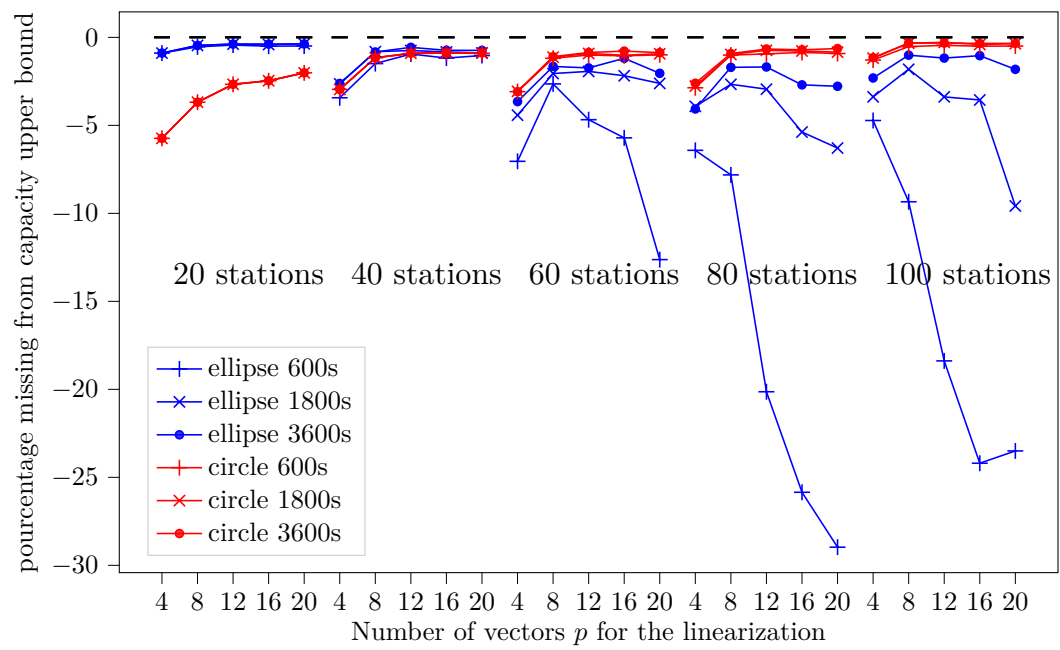


Figure 15: Results for high density instances

d \ time (s)	600	1800	3600
30	40	60	80
70	20	40	40

Table 1: Maximal number of stations for which EL has a better mean objective function than CL

stations, the EL model really benefits from extra computation time whereas the CL model doesn't need more than 600 seconds. So, when the instance size does not exceed 80 stations and when sufficient CPU time is allowed, the EL model outperforms the CL model. Another noticeable trend is that high density instances are far closer to the naive upper bound (the majority of the solutions are between 0 and 5 % away from it), while low density instances are seldom at less than 5 % of difference. As before, the combinatorics is the key to understand that point: higher density leads to more possible covered stations by a beam. It is also visible that the objective value obtained with the circle model are lower than for the ellipse model for small number of stations, and higher for a high number. It can be explained by the size of the EL model that becomes unmanageable with a high number of stations. Indeed, the number of binary variables and constraints increases faster in the EL model than in the CL model. It is due to the different orientations and elongations allowed for ellipses.

Table 1 shows the maximum number of stations for which the EL model gives better mean results than the CL model, depending on the density and the time limit. For high density, the EL is the best for 40 stations and less, while it is better than the CL model with up to 80 stations for a low density and a time limit of 3600 seconds. This can be interpreted by considering that the elliptic beams are more efficient to capture users spread in less dense areas, while circular beams are sufficient for highly dense areas. This would also suggest an adaptative selection of elliptic or circular beams depending on the density of the subareas to be covered.

Table 2 gives indications on the impact of numbers of scalar product p for the linearization. The number of times a certain value of p gives better mean results than the other values of p depending on the model is shown. The * express that for two instances, the mean results for 16 and 20 scalar products are the same after rounding the mean objective value to the thousandth. This shows that the size of the EL model makes it less efficient for a number of scalar product p higher in the linearization.

Overall this application shows that, under the above-described allotted CPU time and problem size limit conditions, the proposed extension of the euclidean norm linearization of [Camino et al., 2019] to elliptic constraints are manageable and allow to obtain significant gain in a practical application.

model \ p	4	8	12	16	20
EL	4	5	12	7	2
CL	0	1	4	11*	16*

Table 2: Number of best means depending on the number of scalar product P used

5 Conclusion

This work about the linearization of non-convex MINLP proposed theoretical and practical results based on the euclidean norm linearization of [Camino et al., 2019]. A linearization of the euclidean norm based on the scalar product between regularly spaced unit vectors and the vector that needs to be measured has been developed. From a theoretical point of view, the guarantee that given any approximation error the linearization method uses the minimum number of pieces has been proven, which means that the model uses polygons with the least number of sides to approximate a circle with a modulable and measurable approximation of nonlinear constraints. Moreover, it has been shown that linearizing elliptic constraints while keeping the previously mentioned guarantee is achievable, thus the linearization method can be applied to a wider range of problems. As for the practical point of view, the elliptic constraint linearization increases the model complexity with respect to the euclidean norm linearization, which makes this linearization useful under CPU time and problem size limit conditions. This work can be followed in many topics. From the theoretical size, one may focus on MINLP linearization and approximation guarantee, for example with piecewise linearization of more general functions of two variables, with the euclidean norm of \mathbb{R}^2 being a case study. From the practical point of view, heuristics and especially matheuristics could be derived from the proposed linearization scheme to handle more efficiently larger problems.

References

- W. P. Adams and H. D. Sherali. A tight linearization and an algorithm for zero-one quadratic programming problems. *Management Science*, 32(10):1274–1290, 1986.
- A. Borghetti, C. D’Ambrosio, A. Lodi, and S. Martello. An MILP approach for short-term hydro scheduling and unit commitment with head-dependent reservoir. *IEEE Transactions on Power Systems*, 23(3):1115–1124, 2008. doi:10.1109/TPWRS.2008.926704.
- J.-T. Camino, S. Mourgues, C. Artigues, and L. Houssin. A greedy approach combined with graph coloring for non-uniform beam layouts under antenna constraints in multibeam satellite systems. In *2014 7th Advanced Satellite Multimedia Systems Conference and the 13th Signal Processing for*

- Space Communications Workshop (ASMS/SPSC), pages 374–381, 2014. doi: 10.1109/ASMS-SPSC.2014.6934570.
- J.-T. Camino, C. Artigues, L. Houssin, and S. Mourgues. Mixed-integer linear programming for multibeam satellite systems design: Application to the beam layout optimization. In 2016 Annual IEEE Systems Conference (SysCon), pages 1–6, 2016. doi: 10.1109/SYSCON.2016.7490613.
- J.-T. Camino, C. Artigues, L. Houssin, and S. Mourgues. Linearisation of euclidean norm dependent inequalities applied to multibeam satellites design. Computational Optimization and Applications, 2019.
- J.-T. Camino, C. Artigues, L. Houssin, and S. Mourgues. MILP formulation improvement with k-means clustering for the beam layout optimization in multibeam satellite systems. Computers Industrial Engineering, 158:DOI doi.org/10.1016/j.cie.2021.107228, 2021.
- E. Camponogara, M. P. de Castro, A. Plucenio, and D. J. Pagano. Compressor scheduling in oil fields. Optimization and Engineering, 12:153–174, 2011.
- J. G. Dunham. Optimum uniform piecewise linear approximation of planar curves. IEEE Transactions on Pattern Analysis and Machine Intelligence, PAMI-8(1):67–75, 1986. doi: 10.1109/TPAMI.1986.4767753.
- C. D’Ambrosio, A. Lodi, and S. Martello. Piecewise linear approximation of functions of two variables in MILP models. Operations Research Letters, 38(1):39–46, 2010. doi: https://doi.org/10.1016/j.orl.2009.09.005.
- B. Geißler, A. Martin, A. Morsi, and L. Schewe. Mixed Integer Nonlinear Programming, chapter Using piecewise linear functions for solving MINLPs, pages 287–314. The IMA Volumes in Mathematics and its Applications, Vol 154, 2012.
- R. B. Hughes and M. R. Anderson. Simplexity of the cube. Discrete Mathematics, 158(1):99–150, 1996. doi: https://doi.org/10.1016/0012-365X(95)00075-8.
- J. Kallrath and S. Rebennack. Cutting ellipses from area-minimizing rectangles. Journal of Global Optimization, 59:405–437, 2014.
- A. B. Keha, I. R. de Farias, and G. L. Nemhauser. Models for representing piecewise linear cost functions. Operations Research Letters, 32(1):44–48, 2004. doi: https://doi.org/10.1016/S0167-6377(03)00059-2.
- L. Liberti, S. Cafieri, and F. Tarissan. Foundations of Computational Intelligence Volume 3, volume 3, chapter Reformulations in Mathematical Programming: A Computational Approach, pages 153–234. Springer, 2009a.
- L. Liberti, N. Maculan, and Y. Zhang. Optimal configuration of gamma ray machine radiosurgery units: The sphere covering subproblem. Optimization Letters, 3:109–121, 2009b.

- L. S. Liberti. Reformulation and Convex Relaxation Techniques for Global Optimization. PhD thesis, Imperial College London, 2004.
- R. Misener, C. E. Gounaris, and C. A. Floudas. Global optimization of gas lifting operations: A comparative study of piecewise linear formulations. Industrial & Engineering Chemistry Research, 48(13):6098–6104, 2009.
- S. U. Nogueve. Piecewise linear bounding of univariate nonlinear functions and resulting mixed integer linear programming-based solution methods. European Journal of Operational Research, 275(3):1058–1071, 2019. doi: <https://doi.org/10.1016/j.ejor.2018.11.021>.
- I. Nowak. Relaxation and Decomposition Methods for Mixed Integer Nonlinear Programming. Birkhäuser, 2005.
- M. Padberg. Approximating separable nonlinear functions via mixed zero-one programs. Operations Research Letters, 27(1):1–5, 2000. doi: [https://doi.org/10.1016/S0167-6377\(00\)00028-6](https://doi.org/10.1016/S0167-6377(00)00028-6).
- S. Rao, M. Tang, and C.-C. Hsu. Multiple beam antenna technology for satellite communications payloads. ACES Journal, 21(3):1054–4887, 2006.
- S. Rebennack and J. Kallrath. Continuous piecewise linear delta-approximations for bivariate and multivariate functions. J Optim Theory Appl, 167:102–117, 2015a.
- S. Rebennack and J. Kallrath. Continuous piecewise linear delta-approximations for univariate functions: Computing minimal breakpoint systems. J Optim Theory Appl, 167:617–643, 2015b.
- S. Rebennack and V. Krasko. Piecewise linear function fitting via mixed-integer linear programming. INFORMS Journal on Computing, 32(2):507–530, 2020. doi: 10.1287/ijoc.2019.0890.
- J. Rosen and P. Pardalos. Global minimization of large-scale constrained concave quadratic problems by separable programming. Mathematical Programming, 34:163–174, 1986.
- R. Rovatti, C. D’Ambrosio, A. Lodi, and S. Martello. Optimistic MILP modeling of non-linear optimization problems. European Journal of Operational Research, 239(3):32–45, 2014.
- A. Santoyo-González and C. Cervelló-Pastor. Latency-aware cost optimization of the service infrastructure placement in 5g networks. Journal of Network and Computer Applications, 114:29–37, 2018.
- H. D. Sherali and W. P. Adams. A Reformulation-Linearization Technique for Solving Discrete and Continuous Nonconvex Problems. Kluwer Academic Publishers, Dodrecht, 1999.

- H. D. Sherali and L. Liberti. Encyclopedia of Optimization, 2nd edn., chapter Reformulation-linearization technique for global optimization, pages 3263–3268. Springer, 2008.
- T. L. Silva and E. Camponogara. A computational analysis of multidimensional piecewise-linear models with applications to oil production optimization. European Journal of Operational Research, 232(3):630–642, 2014. doi: <https://doi.org/10.1016/j.ejor.2013.07.040>.
- E. Smith and C. Pantelides. A symbolic reformulation/spatial branch-and-bound algorithm for the global optimisation of nonconvex MINLPs. Computers & Chemical Engineering, 23(4):457–478, 1999. doi: [https://doi.org/10.1016/S0098-1354\(98\)00286-5](https://doi.org/10.1016/S0098-1354(98)00286-5).
- W. D. Smith. A lower bound for the simplicity of then-cube via hyperbolic volumes. European Journal of Combinatorics, 21(1):131–137, 2000. doi: <https://doi.org/10.1006/eujc.1999.0327>.
- S. Sridhar, J. Linderoth, and J. Luedtke. Locally ideal formulations for piecewise linear functions with indicator variables. Operations Research Letters, 41(6): 627–632, 2013. doi: <https://doi.org/10.1016/j.orl.2013.08.010>.
- F. Tardella. Existence and sum decomposition of vertex polyhedral convex envelopes. Optimization Letters, 2:363–375, 2007.
- J. P. Vielma and G. L. Nemhauser. Modeling disjunctive constraints with a logarithmic number of binary variables and constraints. Mathematical Programming Serie A, 128:49–72, 2011.
- H. Zhang and S. Wang. Linearly constrained global optimization via piecewise-linear approximation. Journal of Computational and Applied Mathematics, 214(1):111–120, 2008. doi: <https://doi.org/10.1016/j.cam.2007.02.006>.
- C. Zhou, A. Mazumder, A. Das, K. Basu, N. Matin-Moghaddam, S. Mehrani, and A. Sen. Relay node placement under budget constraint. In Proceedings of the 19th International Conference on Distributed Computing and Networking, pages 1–11, 2018.